



## Article

# Experimental Study on the Horizontal Bearing Characteristic of a Strip-Walled Underground Diaphragm Wall

Guoqing Du <sup>1</sup>, Shuang Xi <sup>2</sup>, Chen Ling <sup>2</sup>, Weian Shi <sup>1</sup>, Xiaojuan Li <sup>2</sup> , Mingxing Zhu <sup>2,\*</sup>  and Shouguo Li <sup>1</sup>

<sup>1</sup> China Energy Engineering Group Anhui Electric Power Design Institute Co., Ltd., Hefei 230061, China; duguoqing@ahedi.com.cn (G.D.); shiwa@ahedi.com.cn (W.S.); lishg@ahedi.com.cn (S.L.)

<sup>2</sup> School of Civil Engineering and Architecture, Jiangsu University of Science and Technology, Zhenjiang 212003, China; 221110901105@stu.just.edu.cn (S.X.); 211110901112@stu.just.edu.cn (C.L.); xiaojuan\_li05@outlook.com (X.L.)

\* Correspondence: mxingzhu@just.edu.cn

**Abstract:** Researching and developing a new type of diaphragm wall foundation can solve the problem that the traditional diaphragm wall structure may not meet the high standards of safety and stability of underground structures in some specific engineering environments. This paper focuses on the horizontal bearing characteristic of a new form of foundation, a strip-walled underground diaphragm wall, through a series of model tests. In the tests, nine plexiglass models with different section sizes, wall spacings and wall heights, as well as loading strategies (horizontal loads along and against the wall in the model), were conducted. The influence of the above factors on the horizontal bearing performance of the foundation and the soil resistance distribution around the wall was studied. The results show that when the horizontal load applied along the wall is greater than 50 N, the growth rate of total displacement at the top of the wall gradually decreases; when a horizontal load is applied against the wall, with a uniform change in wall height, the optimal wall spacing is 11 cm. When the same displacement occurs, the bearing performance of the model under the former loading strategy is generally 10% higher than that under the later loading strategy. In addition, the depth where the maximum bending moment along the wall occurred gradually moves downward with the increase in horizontal load, and the increase in wall spacing and wall height has a positive effect on the horizontal bearing characteristic. With the application of load, the maximum bending moment of the wall will gradually decrease along the depth. The increase in wall spacing and wall height can improve the overall flexural stiffness and horizontal bearing performance of the foundation. Lastly, the group wall effect coefficient,  $\beta$ , is put forward, and a simplified formula for calculating the horizontal bearing capacity of a strip wall foundation is proposed. In the formula,  $\beta$  is negatively correlated with the buried depth of the wall and positively correlated with the distance between the walls, and its coefficient is greater than 1.

**Keywords:** strip-walled underground diaphragm wall; model test; horizontal bearing characteristic; group wall effect coefficient



**Citation:** Du, G.; Xi, S.; Ling, C.; Shi, W.; Li, X.; Zhu, M.; Li, S. Experimental Study on the Horizontal Bearing Characteristic of a Strip-Walled Underground Diaphragm Wall. *Buildings* **2024**, *14*, 1637. <https://doi.org/10.3390/buildings14061637>

Academic Editor: Boumediene Nedjar

Received: 10 May 2024

Revised: 28 May 2024

Accepted: 31 May 2024

Published: 3 June 2024



**Copyright:** © 2024 by the authors. Licensee MDPI, Basel, Switzerland. This article is an open access article distributed under the terms and conditions of the Creative Commons Attribution (CC BY) license (<https://creativecommons.org/licenses/by/4.0/>).

## 1. Introduction

Ground wall foundations have the advantages of fast construction speed, good anti-seepage performance, high economic benefit, large overall stiffness, various layout types, etc. They have been commonly used as supporting structures, and now, they are gradually being used as ground wall foundations to bear the upper load. The underground diaphragm wall is often used as a support structure in deep foundation pits, and the deformation characteristics of the system have been studied and applied often [1–7]. The engineering example of their use as an anchoring foundation for bridges has been applied in foreign countries [8,9]. In recent years, the underground diaphragm wall foundation has been used as the anchoring foundation many times in various large-scale bridge projects in China,

gradually replacing the traditional foundation form [10]. However, with the continuous progress in many fields, such as civil engineering, hydraulic engineering and underground engineering, regulations on the safety, stability and construction efficiency of underground structures have become increasingly strict. In some specific engineering environments, the traditional ground wall structure cannot meet these high standards. In view of this, the research and development of new ground wall structures is increasingly important.

This paper proposes a new type of strip wall foundation that can effectively resist soil pressure and superstructure load, has significant horizontal bearing capacity and has good economic benefits. The strip-walled underground diaphragm wall (SUDW) is a new type of anchorage foundation. Its structure is composed of multiple parallel walls under a cap, as shown in Figure 1. In Figure 1,  $D$  is the height of the wall below the bearing platform;  $B$  is the thickness of the wall;  $C$  is the distance between adjacent walls and  $W$  is the width of the wall.

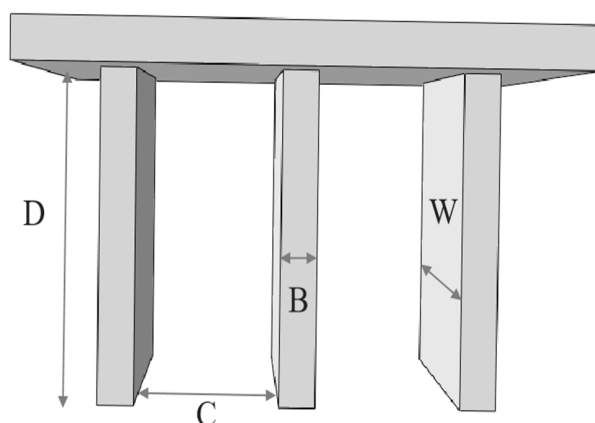


**Figure 1.** The strip-walled underground diaphragm wall foundation.

The results of the research conducted by Zhang et al. [11] show that the horizontal load will have an obvious impact on the bearing performance of the foundation. Previous studies mainly focus on the monolithic ground wall and the closed ground wall [12–18]. Thus, there is still a lack of sufficient theoretical and experimental research on ground wall foundations composed of multiple walls. In particular, the load-bearing characteristics, wall–foundation interaction, the group wall effect reduction coefficient of the foundation and the ultimate load-bearing performance of the foundation still lack sufficient understanding and in-depth research. At present, the research on the load-bearing function of SUDWs as foundations is still in the initial stage. The Canakkale Bridge in Turkey is the only example of SUDWs being used as foundations [19]. The anchoring foundation of the bridge has a unique design. Seven rows of SUDWs are arranged vertically at the lower part of the bridge. Each wall has a plane length of 51.5 m, a thickness of 1.2 m and a depth of more than 20 m, as shown in Figure 2. This innovative design is challenging because each SUDW has to withstand the enormous horizontal tension generated by the suspension bridge cables. Despite many technical difficulties, the successful usage of strip walls in the Canakkale Bridge undoubtedly provides a demonstration in the field of foundation engineering. However, there are no detailed literature reports or in-depth research on the bearing characteristics of this new type of infrastructure. The interaction between the foundation and the soil is a key point in the study of foundation design and protection measures [20]. Therefore, more theoretical research and field tests are still needed for the further application and development of strip ground wall foundations in foundation engineering.

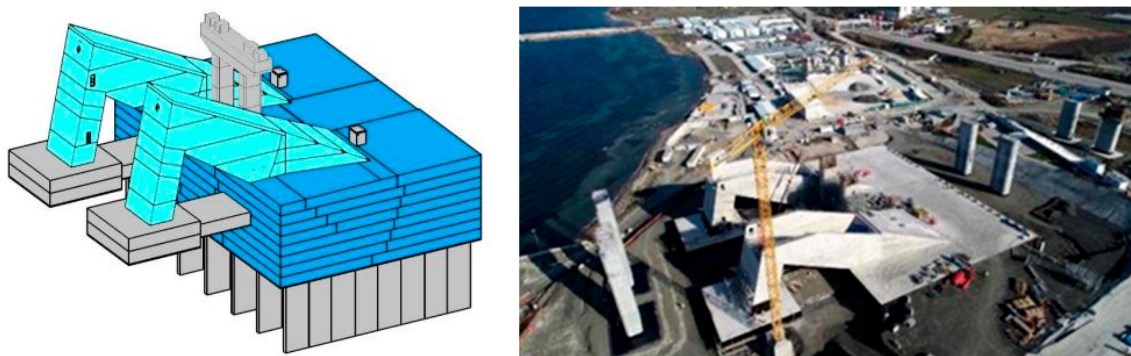


**Figure 2.** 1915 Canakkale Bridge strip wall foundation (Turkey).

Based on the above studies, this paper focuses on the horizontal bearing characteristic of SUDWs using a series of model tests of SUDWs. This paper discusses the variation law of the horizontal ultimate bearing capacity and the internal force of the wall body and proposes the group wall effect coefficient and its fitting formula under the horizontal load by comparing it with the single wall limit load. Based on the group wall effect coefficient, a simplified calculation method of the horizontal bearing capacity of the strip foundation is proposed, which provides a test support and design reference for the study of a new type of SUDW foundation.

## 2. Model Overview

This research test was carried out in a  $1\text{ m} \times 1\text{ m} \times 1\text{ m}$  model box, as shown in Figure 3. Fujian standard sand was selected for the model test, for which the model box was filled with sand in layers. The parameters of the sand were obtained through conventional soil physical tests such as the drying test and the hammer test, as shown in Table 1.



**Figure 3.** Physical photograph of the model box.

**Table 1.** Geotechnical parameters of Fujian standard sand.

Soil Characteristics	Parameter Values
Average particle size $D_{50}$ (mm)	0.17
Maximum dry weight $\gamma_{\min}$ ( $\text{kN}/\text{m}^3$ )	1.638
Minimum dry weight $\gamma_{\max}$ ( $\text{kN}/\text{m}^3$ )	1.349
Specific gravity of soil particles $G_s$	2.632
Relative density $D_r$	52%

The model size of the ground wall was mainly determined according to the size of the existing model box and the boundary effect. The model is made of roughened plexiglass material because interface roughness has more or less of an impact on the shear strength of the sand–structure contact surface [21]. Strain gauges are used and attached on both sides of the wall to collect the strain of the wall, and grooves are used symmetrically on both sides to avoid damaging the wires connected to the strain gauges during loading. Then, holes are drilled on the tops of the caps to pass the wires through the wall groove and lead out of the cap holes. The wall body and cap are attached with strong acrylic glue to ensure the underground diaphragm wall model has a large connection stiffness and good integrity. The thickness of the plexiglass wall is 10 mm, and the elastic modulus of the plexiglass measured by the test is about 2.2 GPa.

In order to study the bearing characteristics of the foundation of walls with different sections, a total of nine plexiglass models with different section sizes were made. The specific model working conditions are shown in Table 2.

**Table 2.** Model conditions.

Sequence No.	Wall Height (cm)	Wall Width (cm)	Aspect Ratio	Wall Spacing (cm)				
1	15	1	15	10				
2	16.5	1	16.5	10				
3	18	1	18	10				
4	15	1	15	11				
5	16.5	1	16.5	11				
6	18	1	18	11				
7	15	1	15	12				
8	16.5	1	16.5 </tr <tr> <td>9</td> <td>18</td> <td>1</td> <td>18</td> <td>12</td> </tr>	9	18	1	18	12
9	18	1	18	12				

### 3. Test Summary

#### 3.1. Test Element Layout

The center of the SUDW is overlapped with the center of the model box, and the lower surface of the cap is flush with the sand surface. The loading device of this test adopts the self-developed servo cylinder loading system with a large stroke and high load. The amplitude of the applied force is from  $-600$  N to  $600$  N, and the amplitude of the applied displacement is 0 to 40 cm.

In the test, five strain gauges are arranged at equal spacing on both sides of each wall to measure the internal force changes in the wall under horizontal load. At the same time, earth pressure boxes are arranged in the center area and edge area of the surface under the bearing and the center of the bottom surface of the three walls. The arrangement of the strain gauges and earth pressure boxes is shown in Figure 4.

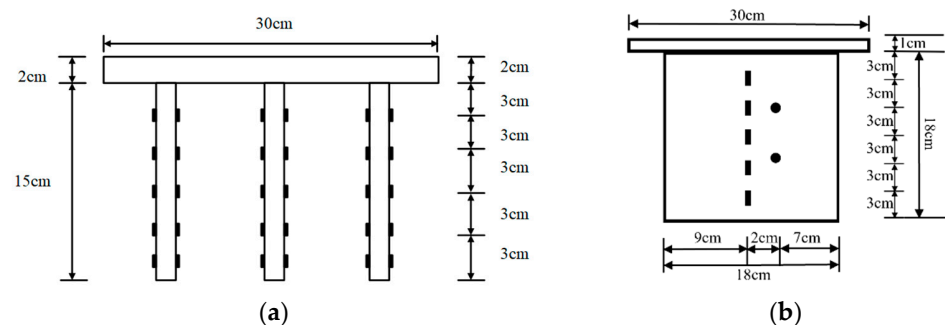


**Figure 4.** Schematic diagram of the layout of the test components. (a) Layout diagram of the strain testing points; (b) layout plan of the earth pressure boxes. Note: black stripes represent strain gauges, and black circles represent earth pressure boxes.

### 3.2. Test Method

The test load is mainly applied through the servo-electric cylinder, which adopts the displacement control mode and controls the test loading force through the change in displacement. A pressure sensor is installed at the end of the guide rod of the servo-electric cylinder to obtain the output force. In order to ensure the accuracy of the loading process, the displacement change speed of the servo cylinder must be strictly controlled during the loading process. In this test, the displacement loading speed is controlled at 0.01 mm/s. In their model test research on the horizontal bearing capacity of a shaft-type underground diaphragm wall, Dai et al. [22] pointed out that when an obvious turning point occurs in the horizontal load–displacement curve, the corresponding force is the horizontal ultimate bearing capacity. Here, the load corresponding to the horizontal displacement of the wall body of 11mm is taken as the horizontal ultimate bearing capacity. The model test loading is shown in Figure 5.

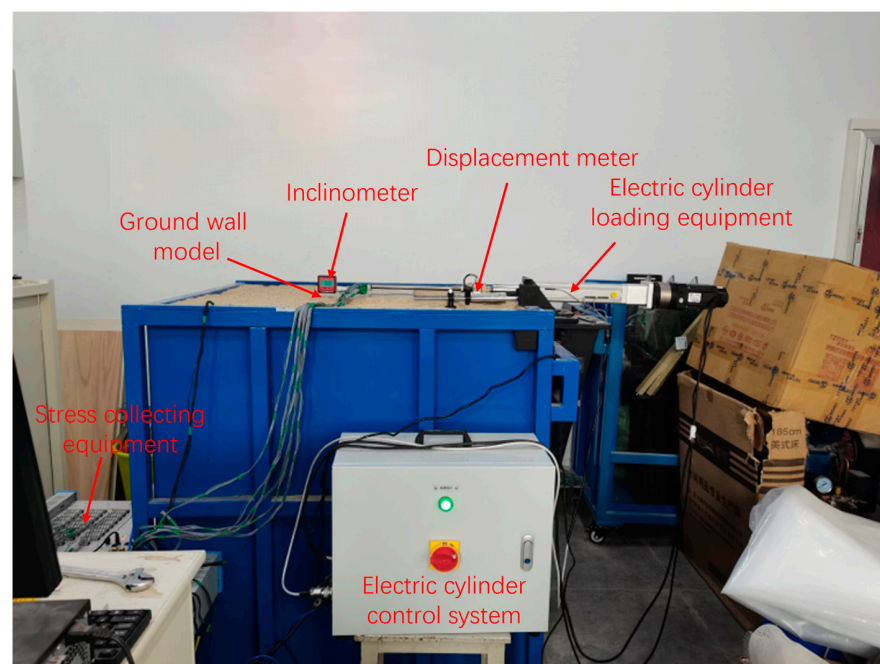


**Figure 5.** Horizontal loading test of the underground continuous wall foundation.

Because of the different directions of the walls, the horizontal loading designed in this experiment is divided into two types, as shown in Figure 6. The first type is horizontal loading, where the direction of the horizontal load is parallel to the wall. The second type is longitudinal horizontal loading, where the direction of the horizontal load is perpendicular to the wall.



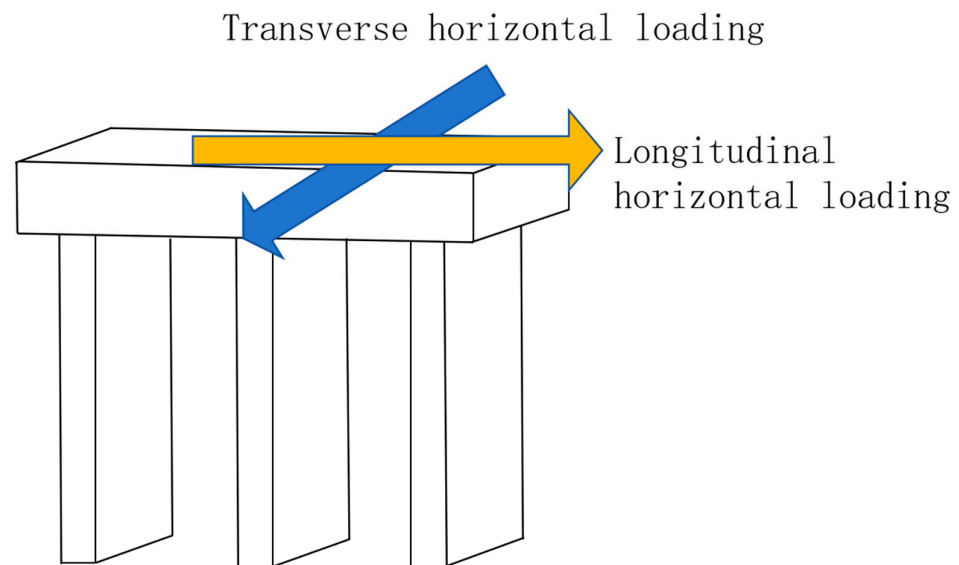


**Figure 6.** Schematic diagram of horizontal and vertical loading.

#### 4. Analysis of Test Results

##### 4.1. Analysis of the Load–Displacement Curve

According to the different wall spacing, wall height and loading direction of the model wall, the load–displacement relationship curve of the wall top is obtained. The load and displacement of the model wall are mainly derived from the feedback of the servo-electric cylinder.

The specific value of the wall bending moment  $M(z)$  cannot be directly measured from the test, and is usually calculated after the strain value is processed. Using the values of tensile strain  $\varepsilon_+$  and compressive strain  $\varepsilon_-$  at the measuring points of each test section obtained in the model test, the corresponding section bending moment is calculated according to the bending strain  $\Delta\varepsilon = \varepsilon_+ - \varepsilon_-$  at the section, where  $B$  is the distance between tensile and compressive symmetric strain measuring points and  $EI$  is the flexural stiffness of the plexiglass material.

$$M = \frac{EI\Delta\varepsilon}{B} \quad (1)$$

##### (1) Q-S curve of the longitudinal horizontal load model wall

For longitudinal horizontal loading, it can be seen in Figure 7 that with an increase in the output load of the servo-electric cylinder, the total displacement first rapidly increases and then slowly increases with the increase in load. The nonlinear characteristics are caused by the gradual plastic state of the model wall as the wall–soil interaction slowly enters the model wall with the increased load. When the load is greater than 50 N, with a further increase in the load, the growth rate of the total displacement of the top of the wall gradually decreases, showing a nonlinear characteristic, which also indicates that the bearing capacity of the foundation soil is relatively high. The wall–soil system as a whole presents a flexible characteristic.

According to Figure 7, for longitudinal horizontal loading, when the wall spacing is 10 cm and 12 cm, the changes in different wall heights have no significant impact on the vertical bearing performance of the ground wall model. However, when the wall spacing is 11 cm, the higher the wall height, the smaller the horizontal displacement under the same load. Under the longitudinal horizontal load, with a uniform change in wall height, it is found that the optimal bearing performance spacing of the ground wall occurs at the wall spacing of 11 cm.

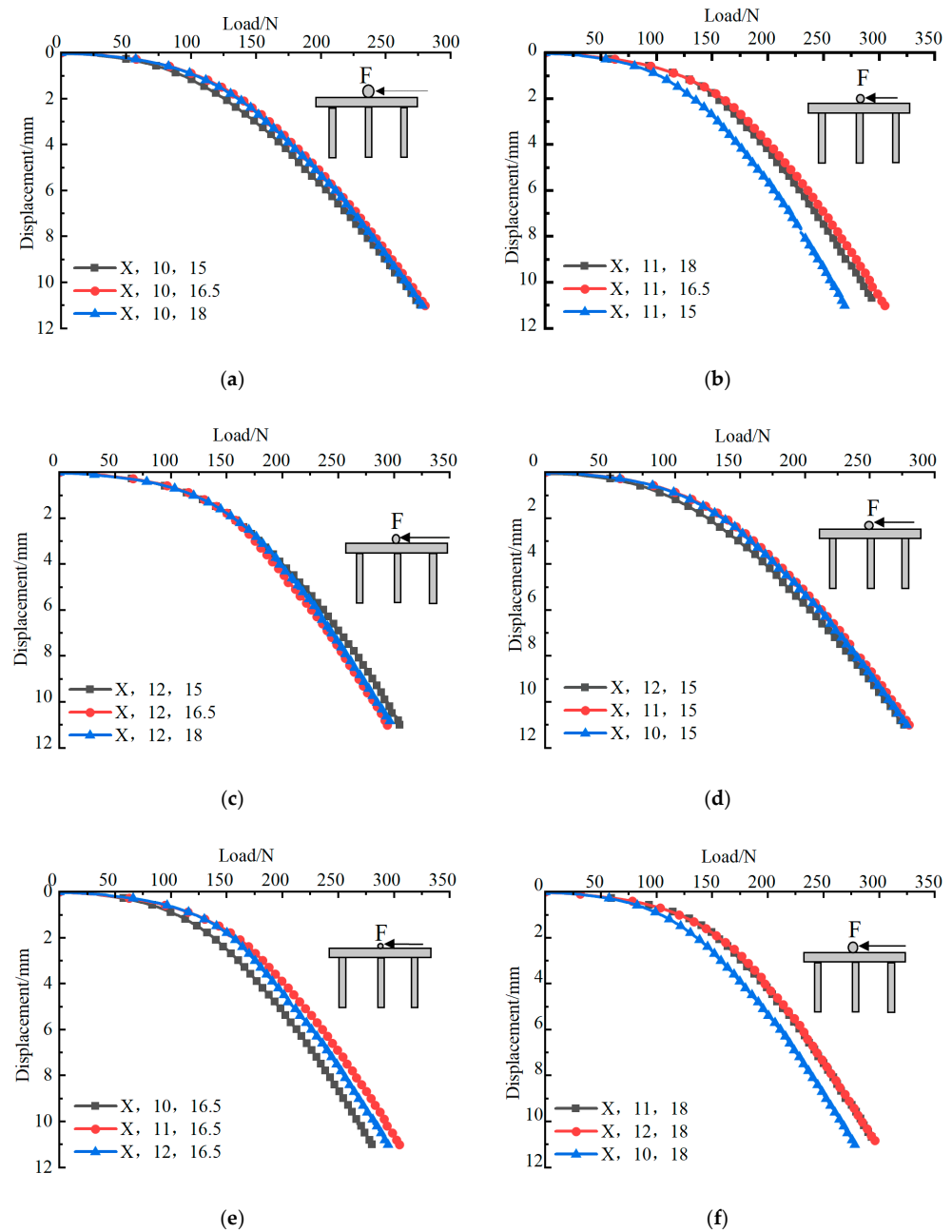


**Figure 7.** Longitudinal horizontal load–displacement curve of the wall top. (a) Wall spacing of 10 cm, different wall heights. (b) Wall spacing of 11 cm, different wall heights. (c) Wall spacing of 12 cm, different wall heights. (d) Wall height of 15 cm, different wall spacings. (e) Wall height of 16.5 cm, different wall spacings. (f) Wall height of 18 cm, different wall spacings. The direction of the arrow indicates the direction of the longitudinal horizontal load.

## (2) Q-S curve of the transverse horizontal load model wall

As shown in Figure 8, under the action of transverse horizontal load, keeping the wall spacing unchanged, increasing the wall height significantly improves its transverse bearing characteristics because increasing the wall height significantly increases the section stiffness at this section. Compared with the same displacement, the corresponding longitudinal horizontal load is generally more than 10% higher than the horizontal load, which is related to the size of the section stiffness of the two, that is, the higher the height of the long side of the ground wall model, the greater the section stiffness and the corresponding bearing performance.

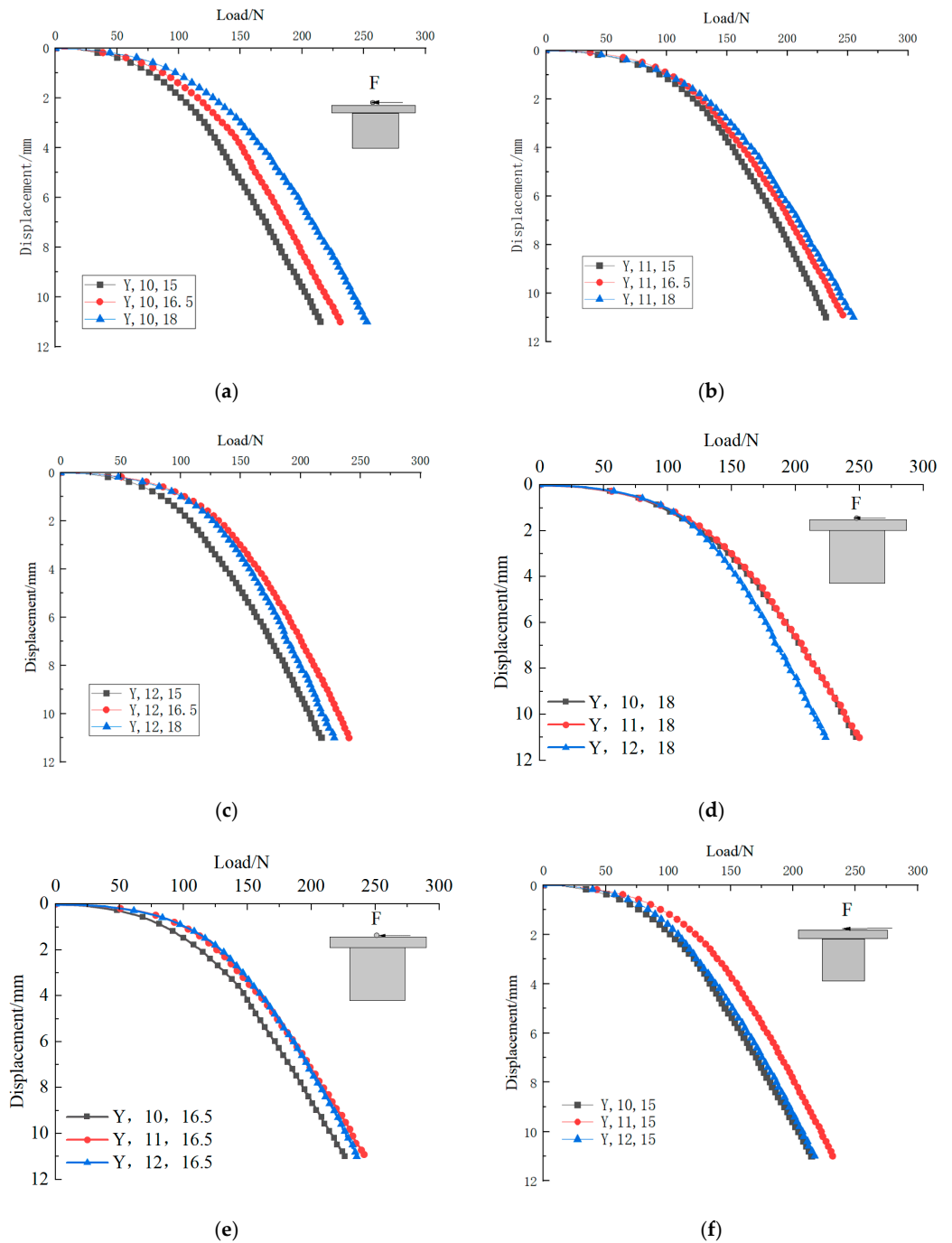


**Figure 8.** Horizontal load–displacement curve of the wall top. (a) Wall spacing of 10 cm, different wall heights. (b) Wall spacing of 11 cm, different wall heights. (c) Wall spacing of 12 cm, different wall heights. (d) Wall height of 15 cm, different wall spacings. (e) Wall height of 16.5 cm, different wall spacings. (f) Wall height of 18 cm, different wall spacings. The direction of the arrow indicates the direction of the transverse horizontal load.

Horizontal and vertical loading show the same phenomenon, which is related to the change in the compactness of the sand in the test, and the gradual hardening of the sand with the progress of the test may lead to this phenomenon. As the method of first burying and then backfilling is adopted in this experiment, the contact tightness between the back-filled sand and the surface under the slab wall model may not be completely consistent each time, which may have a certain influence on the variation law of the ultimate bearing capacity of the foundation of the ground wall.



#### 4.2. Influence of Wall Buried Depth on Longitudinal Horizontal Loading Performance

When the bottom of the cap is flush with the mud surface and the loading mode is longitudinal horizontal loading, the bending moment buried depth curves of the three walls when the wall spacing is 10 cm and the wall buried depth is 15 cm, 16.5 cm and 18 cm are shown in Figure 9.

The following can be seen in Figure 9: (1) When the buried depth of the wall increases, the load value exerted by the wall to reach the longitudinal horizontal ultimate bearing capacity is larger, and the overall bending moment value increases with the increase in the buried depth of the wall. (2) When the longitudinal horizontal load value increases, the absolute change in the bending moment also increases. The main reason is that the deformation of the wall gradually increases with the increase in the applied load, so the soil reaction on the wall–soil contact surface also increases, resulting in an increase in the internal force of the wall section. (3) With the application of longitudinal horizontal load, the ground wall model overturns because of translational plus rotation, which makes the upper cap of the left wall and the soil contact and squeeze each other and has a certain disturbance influence on the soil. It can be seen in Figure 9a,d,e that the bending moment distribution law of the three figures is roughly the same, and the bending moment value of the pile body increases with the increase in depth in all cases. After reaching the maximum bending moment value, the bending moment gradually decreases with the increase in depth. (4) As shown in Figure 9a, there are three approximately equal bending moment values near the bottom of the wall, which may be caused by the uneven filling of the test soil. The negative bending moment phenomenon shown in Figure 9e may be because the connector of the bearing table is not tightly connected, which has a certain negative bending moment effect on the adjacent wall body but does not affect the maximum bending moment value of the wall body in general. The design of the connector needs to be improved in the course of subsequent research to reduce the impact of negative bending moments.

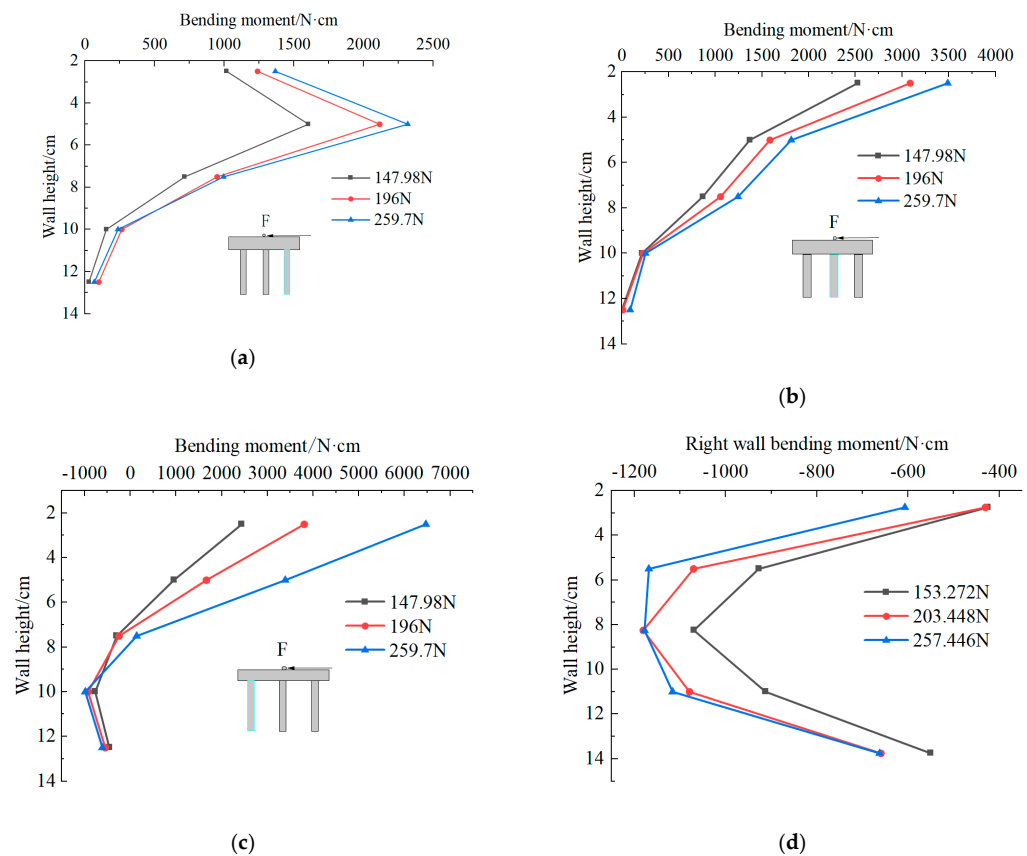
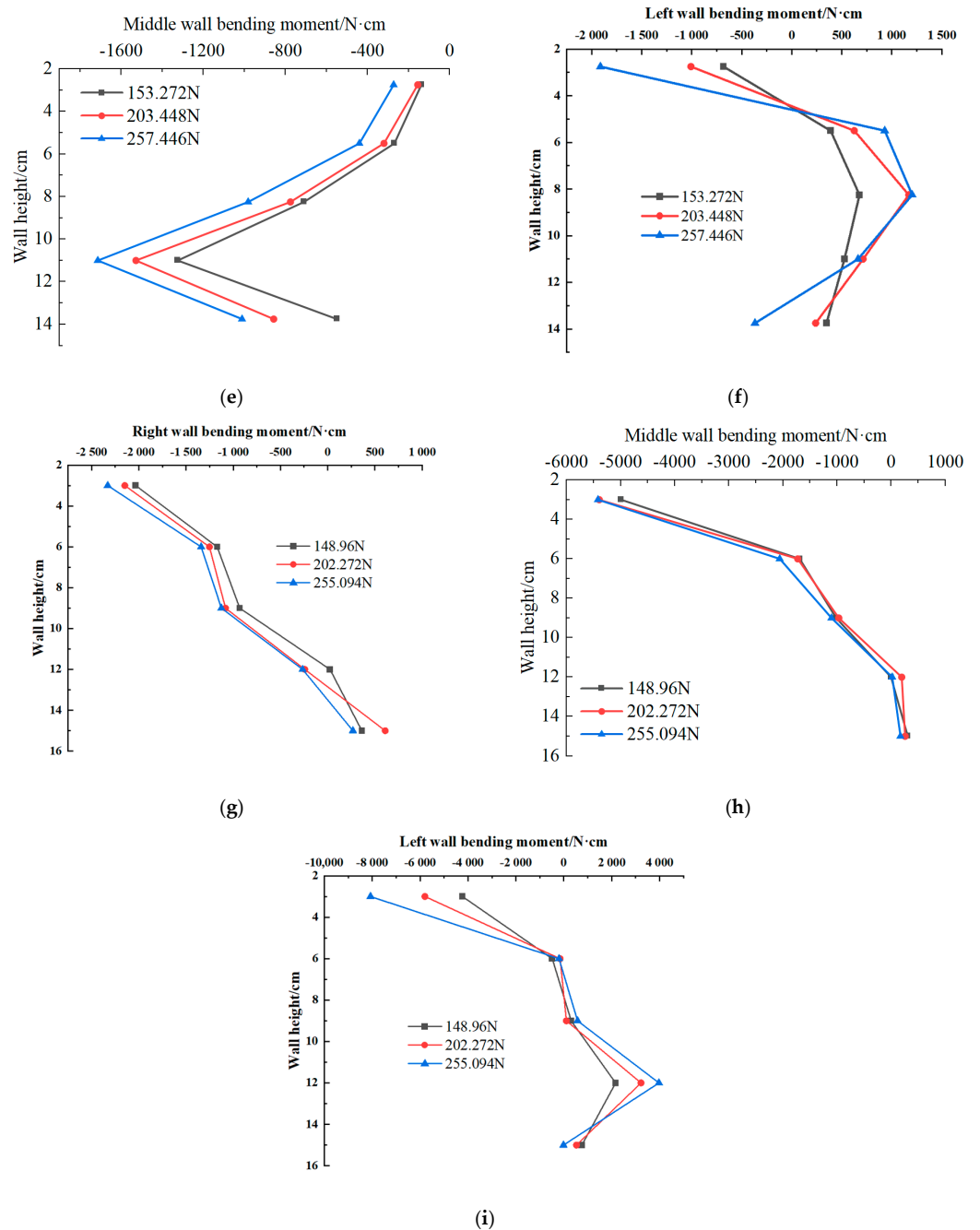


Figure 9. Cont.



**Figure 9.** Longitudinal horizontal loading bending moment changes with burial depth. (a) The bending moment of the right wall varies with the buried depth of 15 cm. (b) The bending moment of the middle wall varies with the buried depth of 15 cm. (c) The bending moment of the left wall varies with the buried depth of 15 cm. (d) Bending moment diagram of the right wall (wall height 16.5 cm). (e) Bending moment diagram of the middle wall (wall height 16.5 cm). (f) Bending moment diagram of the left wall (wall height 16.5 cm). (g) Bending moment diagram of the right wall (wall height 18 cm). (h) Bending moment diagram of the middle wall (wall height 18 cm). (i) Bending moment diagram of the left wall (wall height 18 cm).

#### 4.3. Influence of Wall Buried Depth on Lateral Horizontal Loading Performance

When the transverse horizontal loading wall spacing is 10 cm and the wall buried depth is 15 cm, 16.5 cm and 18 cm, the bending moment buried depth curves of the three walls are shown in Figure 10.

Based on Figure 10, it can be concluded that (1) when the buried depth of the wall increases, the load value exerted by the wall to reach the lateral ultimate bearing capacity increases, which has a certain relationship with the substantial increase in the stiffness of the section. (2) When the transverse horizontal load value increases, the absolute change in the bending moment also increases. The main reason is that the deformation of the wall gradually increases with the increase in the applied load, and the soil reaction on the wall–soil contact surface also increases, which leads to the increase in the internal force of the wall section. (3) The negative bending moment phenomenon in the figure may be be caused by the improper degree of embeddedness of the connector. (4) The phenomenon of inconsistent bending moment values on both sides of the wall may be caused by the eccentric load caused by the flexible material of the model wall itself and the position of the loading point, which is not strictly centered.

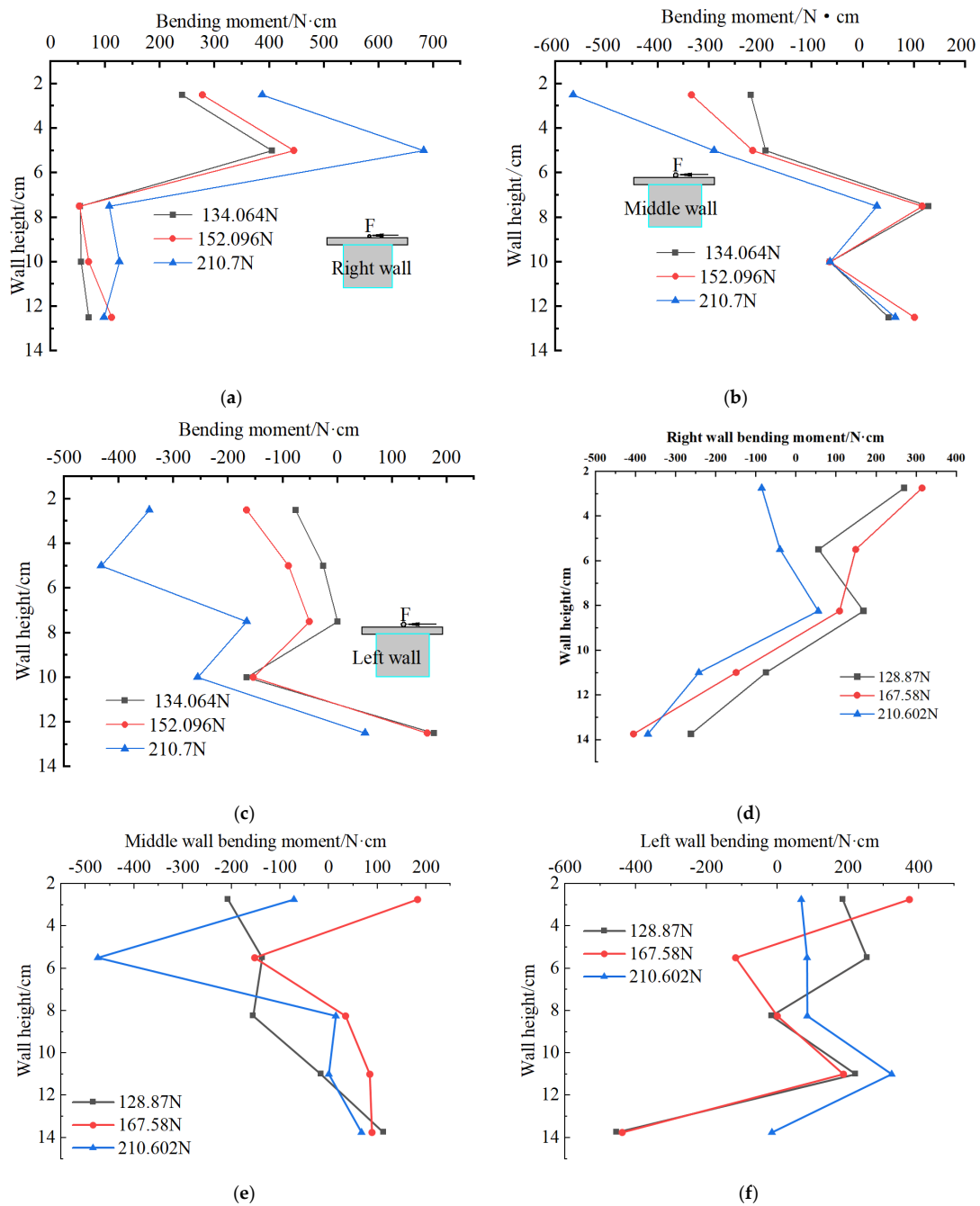
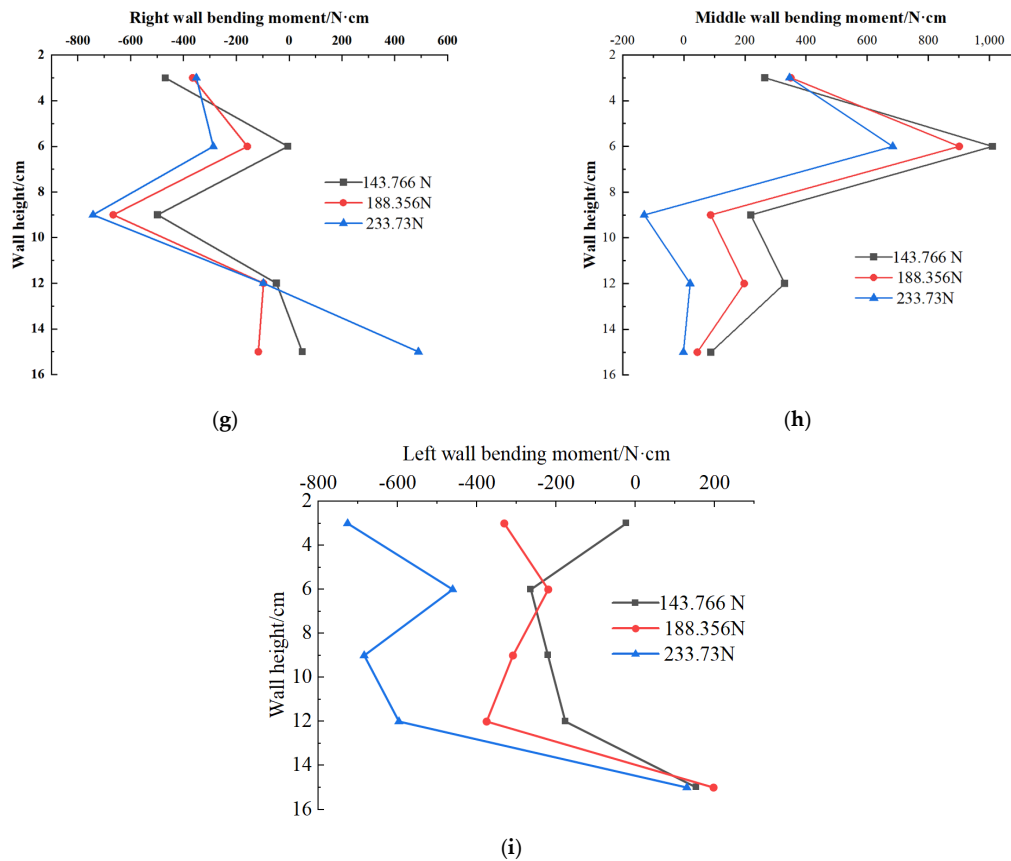


Figure 10. Cont.



**Figure 10.** Lateral horizontal loading bending moment changes with burial depth. (a) Bending moment diagram of the right wall (wall height 15 cm). (b) Wall bending moment diagram (wall height 15 cm). (c) Bending moment diagram of the left wall (wall height 15 cm). (d) Bending moment diagram of the right wall (wall height 16.5 cm). (e) Bending moment diagram of the middle wall (wall height 16.5 cm). (f) Bending moment diagram of the left wall (wall height 16.5 cm). (g) Bending moment diagram of the right wall (wall height 18 cm). (h) Bending moment diagram of the middle wall (wall height 18 cm). (i) Bending moment diagram of the left wall (wall height 18 cm).

#### 4.4. Influence of Wall Buried Depth on Lateral Horizontal Loading Performance

When the vertical horizontal loading wall height is 18 cm and the wall spacing is 10 cm, 11 cm and 12 cm, the bending moment buried depth curves of the three walls are shown in Figure 11.

Based on Figure 11a,d, it can be concluded that (1) when the wall spacing increases, the load value exerted by the wall to reach the longitudinal horizontal ultimate bearing capacity is larger, so the overall bending moment value increases with the increase in the wall spacing. (2) When the longitudinal horizontal load value increases, the absolute change in the bending moment also increases. The main reason is that the deformation of the wall gradually increases with the increase in the applied load, and the soil reaction on the wall–soil contact surface also increases, which leads to the increase in the internal force of the wall section. (3) In Figure 11b–e, h, it can be seen that the bending moment distribution rules of these four figures are roughly the same, and the bending moment gradually decreases with the increase in depth. This is because with the increase in the vertical horizontal load, the lateral constraint of the soil becomes stronger, and the shear force decays rapidly, resulting in the bending moment at the bottom of the wall being almost 0. (4) When the external loads presented in Figure 11d,g are similar, the interaction force between wall and soil can be significantly increased by increasing the wall spacing, and the bending moment value of the wall body decreases with the increase in the wall spacing. As shown in Figure 11a,d, increasing the wall spacing improves the longitudinal horizontal bearing

capacity, and the bending moment bearing performance in the longitudinal horizontal direction is also further improved. This is because the close contact between the soil and the model under the action of load can be regarded as a rigid body. The increase in the wall spacing strengthens the interaction force between the soil and the foundation model, thus increasing the overall stiffness and improving the longitudinal horizontal bearing performance of the model.

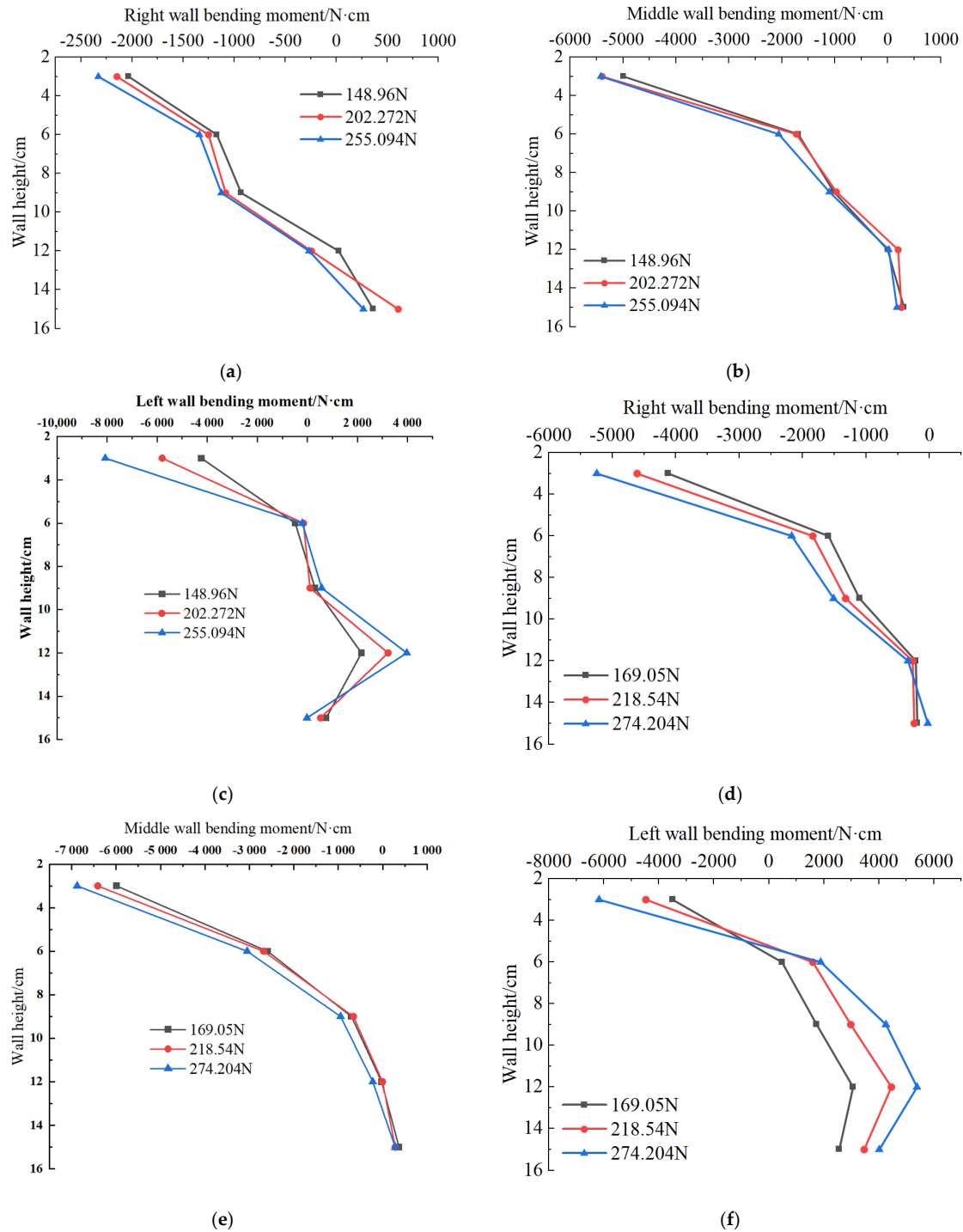
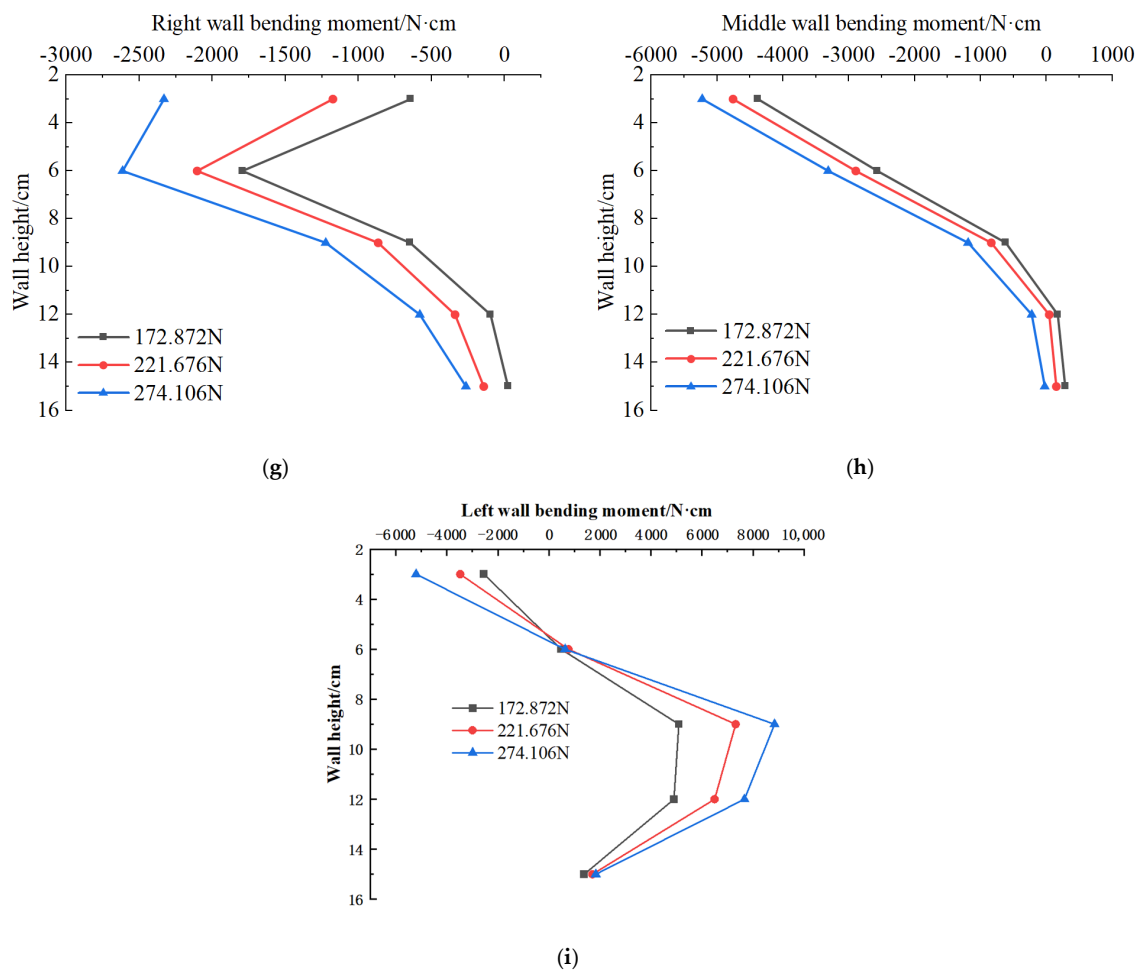


Figure 11. Cont.



**Figure 11.** Longitudinal horizontal loading bending moment changes with wall spacing. (a) Right wall bending moment diagram (spacing 10 cm). (b) Middle wall bending moment diagram (spacing 10 cm). (c) Left wall bending moment diagram (spacing 10 cm). (d) Right wall bending moment diagram (spacing 11 cm). (e) Middle wall bending moment diagram (spacing 11 cm). (f) Left wall bending moment diagram (spacing 11 cm). (g) Right wall bending moment diagram (spacing 12 cm). (h) Middle wall bending moment diagram (spacing 12 cm). (i) Left wall bending moment diagram (spacing 12 cm).

#### 4.5. Influence of Wall Buried Depth on Lateral Horizontal Loading Performance

When the wall height is 15 cm and the wall spacing is 10 cm, 11 cm and 12 cm respectively, the bending moment buried depth curves of the three walls are shown in Figure 12.

The following can be concluded from Figure 12: (1) When the wall spacing increases, the load value exerted by the wall to reach the horizontal ultimate bearing capacity is larger, so the overall bending moment value increases with the increase in the wall spacing. (2) When the transverse horizontal load value increases, the absolute change in the bending moment also increases. The main reason is that the deformation of the wall gradually increases with the increase in the applied load, and the soil reaction on the wall–soil contact surface also increases, which leads to the increase in the internal force of the wall section. (3) Increasing the wall spacing improves the horizontal bearing capacity, and the bending moment bearing performance in the horizontal direction is also further improved. This is because the close contact between the soil and the model under load can be regarded as a rigid body. The increase in the wall spacing increases the overall contact tightness, increases the overall stiffness of the foundation, and improves the horizontal bearing performance of the model. (4) The soil mass is in a relatively elastic condition under the action of a small load on the top of the wall. With the application of a load, the soil mass devel-



ops from elasticity to plasticity, and its plastic region gradually moves deeper to resist the action of horizontal load, while the maximum bending moment also moves downward.

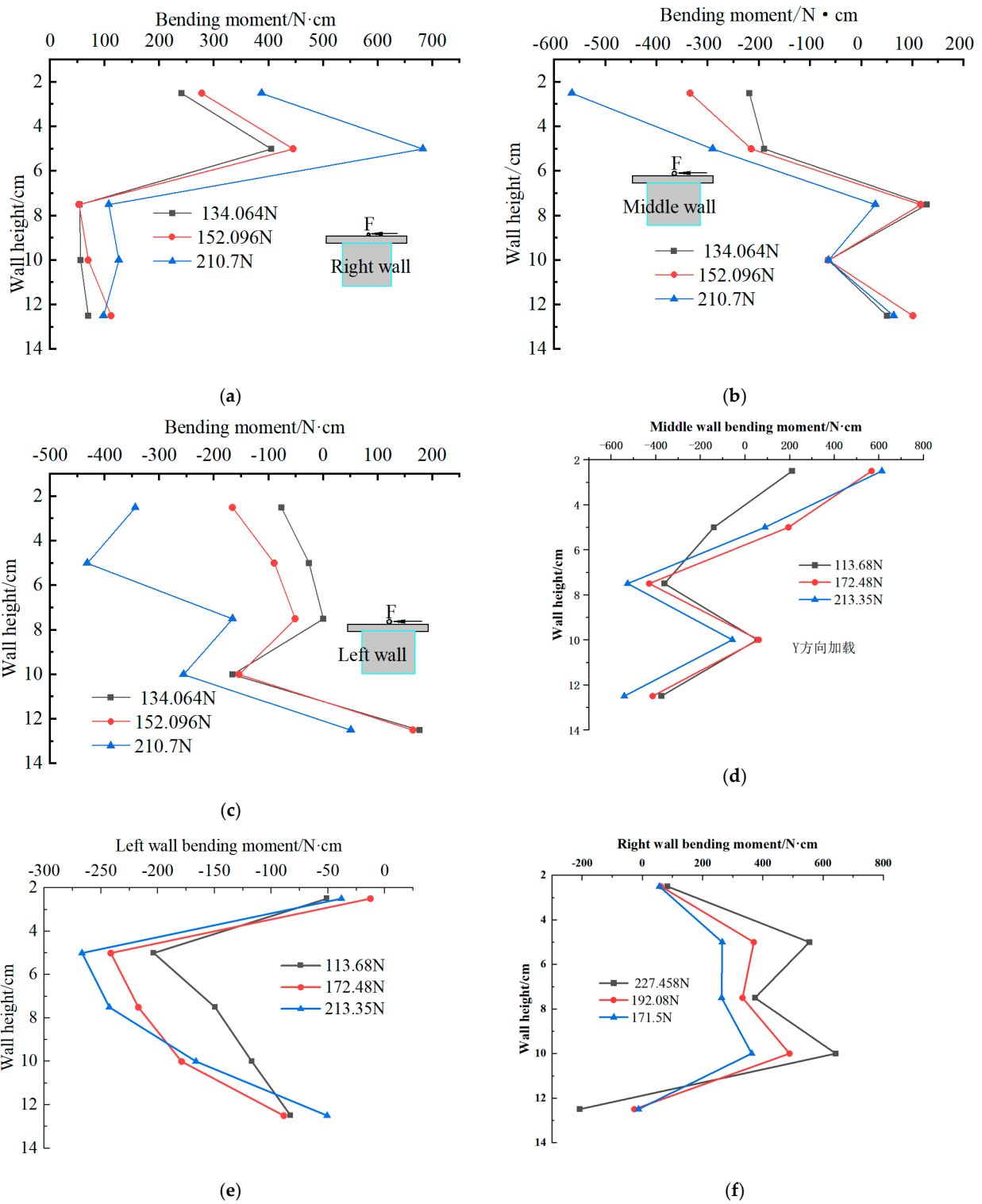
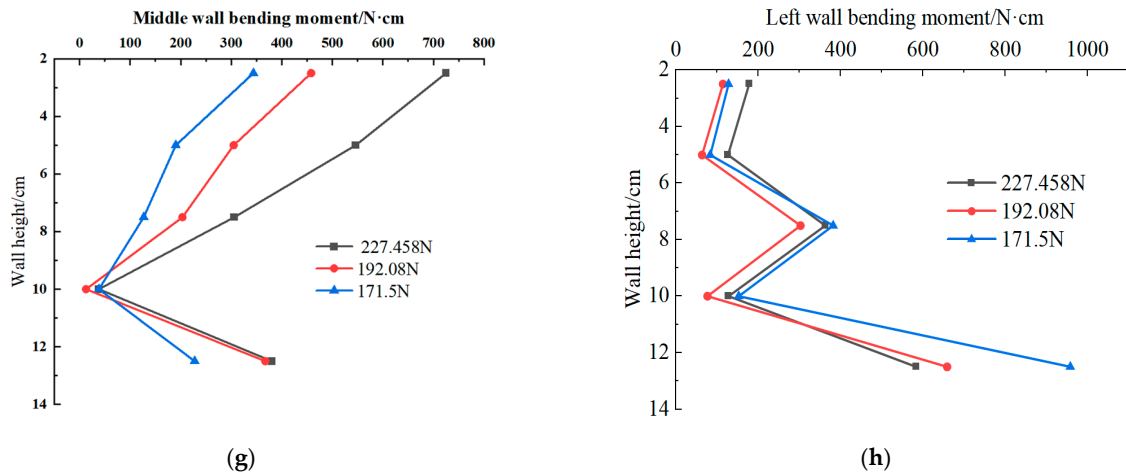


Figure 12. Cont.



**Figure 12.** Variation in transverse horizontal loading bending moment with wall spacing. (a) Bending moment diagram of the right wall (buried depth 10 cm). (b) Bending moment diagram of the middle wall (buried depth 10 cm). (c) Bending moment diagram of the left wall (buried depth 10 cm). (d) Bending moment diagram of the right wall (buried depth 16.5 cm). (e) Bending moment diagram of the left wall (buried depth 16.5 cm). (f) Bending moment diagram of the right wall (buried depth 18 cm). (g) Bending moment diagram of the middle wall (buried depth 18 cm). (h) Bending moment diagram of the left wall (buried depth 18 cm).

#### 4.6. The Group Wall Effect Coefficient under Horizontal Load

The load value corresponding to an 11 mm displacement of a single wall and an 11 mm horizontal displacement of a group wall are compared and analyzed to study the group wall effect coefficient of three walls with bearing caps under horizontal load. The horizontal load–displacement curves of a monolithic wall with different wall heights are shown in Figure 13.

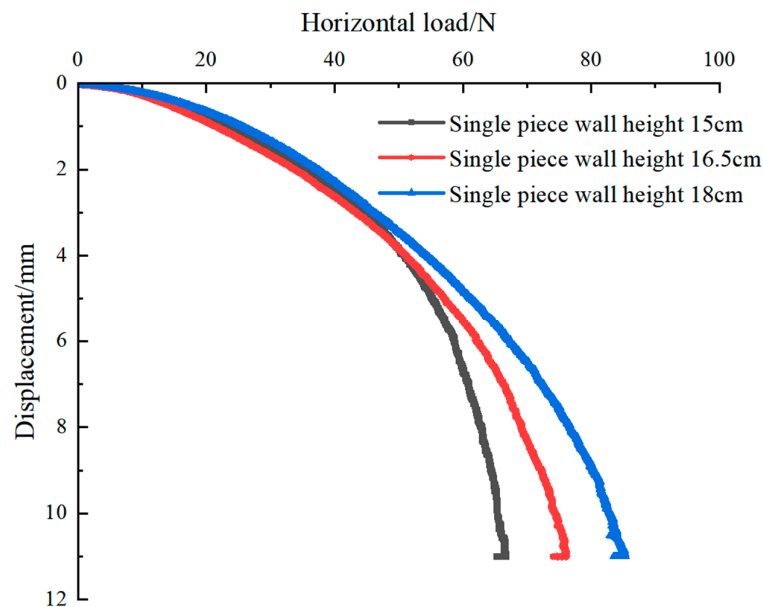


**Figure 13.** Horizontal load–displacement diagram of a monolithic wall.

In Table 3,  $H_t$  represents the horizontal bearing capacity of three walls and caps together, and  $H_s$  is the horizontal bearing capacity of a single wall strip.  $\beta = H_t/(n \times H_s)$ , where  $n$  represents the number of walls ( $n = 3$ ). As can be seen in Table 3, when the bottom of the cap is level with the mud surface, as the buried depth of the foundation increases from 15 cm to 16.5 cm and 18 cm, the horizontal group wall effect coefficient  $\beta$  of the founda-

tion decreases from 1.38 to 1.24 and 1.09. This indicates that the buried depth is negatively correlated with the group wall effect coefficient of the foundation under the cap when other factors remain unchanged. At the same time, it can be seen in Table 3 that as the wall spacing of the model increases from 10 cm to 11 cm and 12 cm, the horizontal group wall effect coefficient  $\beta$  of the foundation increases from 1.09 to 1.1620 and 1.1624, indicating that the wall spacing is positively correlated with the group wall effect coefficient of the foundation under the bearing table when other factors remain unchanged.

**Table 3.** Group wall effect coefficients of three walls under horizontal load.

ID	$D/B$ (Wall Height/Wall Width)	$C/B$ (Wall Spacing/Wall Width)	Comparison of Horizontal Bearing Capacity	Horizontal Group Wall Effect Coefficient $\beta$
1	15	10	65.268/270.48	1.38
2	15	11	65.268/263.62	1.35
3	15	12	65.268/298.9	1.53
4	16.5	10	74.088/274.596	1.24
5	16.5	11	74.088/298.9	1.35
6	16.5	12	74.088/288.12	1.30
7	18	10	83.496/272.44	1.09
8	18	11	83.496/291.06	1.16
9	18	12	83.496/291.158	1.16

Parameter fitting is a challenging task that can be implemented with more precise analysis methods such as the YOLO network [23]. However, because of limitations in article length, the separation of variables method is adopted for coefficient fitting. By observing the data in Table 3, it can be seen that the horizontal group wall effect coefficient  $\beta$  is related to the buried depth/wall thickness ( $D/B$ ) and the wall spacing/wall thickness ( $C/B$ ), and it is more significantly affected by the buried depth/wall thickness ( $D/B$ ). Therefore, the relationship between the group wall effect coefficient  $\beta$  and the change in the buried depth/wall thickness ( $D/B$ ) is first fitted. Then, fitting the relationship between it and wall spacing/wall thickness ( $C/B$ ) can effectively reduce the error of the fitting formula. The specific operation is as follows:

$$\beta = f(D/B)g(C/B) \quad (2)$$

where ( $D/B$ ) is the influence coefficient of the relationship between wall depth and wall thickness on the effect coefficient of the horizontal group wall.  $g(C/B)$  is the influence coefficient of the relationship between wall spacing and wall thickness on the wall effect coefficient of the horizontal group.

First, scatter plots are drawn with the buried depth/wall thickness ( $D/B$ ) values of each group of tests in Table 3 as the horizontal coordinate and the  $\beta$  value of the horizontal group wall effect coefficient as the vertical coordinate. As can be seen from Figure 14, there is a relatively obvious linear relationship between the two. The function relationship between the  $\beta$  of the horizontal group wall effect coefficient and the buried depth/wall thickness ( $D/B$ ) is obtained by fitting logarithmic data points:

$$\beta = -0.094 \left( \frac{D}{B} \right) + 2.835 \quad (3)$$

If Formula (3) is substituted into (2), we obtain:

$$\beta = \left[ -0.094 \left( \frac{D}{B} \right) + 2.835 \right] g(C/B) \quad (4)$$

The data in Table 3 are processed, and the scatter plot shown in Figure 15 is drawn with the value of  $\beta/[-0.094(D/B) + 2.835]$  as the vertical coordinate and the value of the

wall spacing/wall thickness ( $C/B$ ) as the horizontal coordinate. The final fitting formula of the horizontal group wall effect coefficient  $\beta$  can be obtained by fitting as follows:

$$\beta = \left[ -0.094 \left( \frac{D}{B} \right) + 2.835 \right] \left[ 0.036 \left( \frac{C}{B} \right) + 0.609 \right] \quad (5)$$

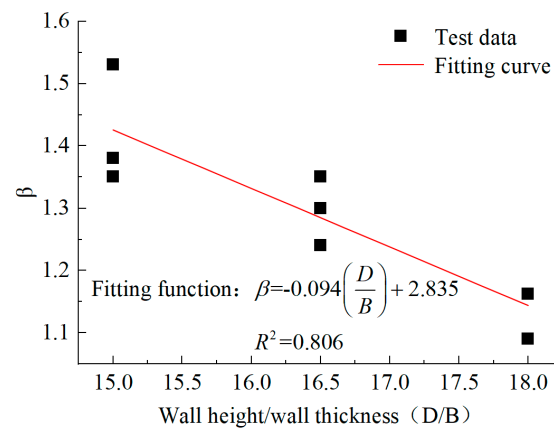


Figure 14. Fitting results of  $\beta$  and ( $D/B$ ).

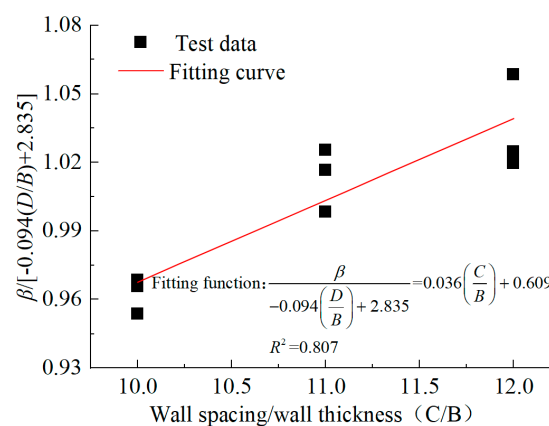


Figure 15. Fitting results of  $\beta$ .

#### 4.7. Simplified Calculation Method for the Horizontal Bearing Capacity of the SUDW Foundation

According to the results of the study on the displacement curve of longitudinal horizontal load and the group wall effect coefficient, a simplified calculation method for the longitudinal horizontal bearing capacity of the foundation under the laboratory test conditions of the ground connecting wall model is proposed in this section as follows:

$$H_t = \beta n H_s \quad (6)$$

where  $H_t$  represents the longitudinal horizontal bearing capacity of the foundation of the connecting wall;  $H_s$  represents the longitudinal horizontal bearing capacity of a single wall;  $n$  is the number of walls; and  $\beta$  is the longitudinal horizontal group wall effect coefficient. The longitudinal horizontal  $\beta$  value is the same as the corresponding group wall effect coefficient under the longitudinal horizontal load mentioned above.

## 5. Conclusions

Based on the laboratory test research of the SUDW model under the influence of different wall spacing and wall height factors, the bearing capacity of the foundation and the internal force distribution law of the wall body of the SUDW model under the horizontal load condition are analyzed. Then, the group wall effect coefficient under the action of

the bearing cap and a simplified calculation method of the horizontal bearing capacity are obtained. The following conclusions are drawn:

(1) Under longitudinal horizontal load, when the load is greater than 50 N, with a further increase in the load, the growth rate of the total displacement of the wall top gradually decreases, showing nonlinear characteristics. Under lateral horizontal load, with the uniform change in the wall height, the optimal bearing performance spacing of the ground connecting wall occurs at the wall spacing of 11 cm. When the same displacement occurs, the corresponding longitudinal horizontal load is generally more than 10% higher than the horizontal load.

(2) When the wall height increases, the load value exerted to reach the horizontal ultimate bearing capacity is larger, and the total bending moment value increases with the increase in the buried depth of the wall. At the same time, when the external load is similar, the bending stiffness can be significantly improved by increasing the wall spacing, and the bending moment value decreases with the increase in the wall spacing.

(3) Based on the comparison with the load–displacement curve of a single piece of wall, an expression of the change in the horizontal group wall effect coefficient with wall spacing and wall height is established. According to the expression, the buried depth of the model wall is negatively correlated with the group wall effect coefficient. As the wall height of the ground connecting the wall increases from 15 cm to 18 cm, the horizontal group wall effect coefficient of the model decreases from 1.38 to 1.09. The model wall spacing is positively correlated with the group wall effect coefficient. When the model wall spacing increases from 10 cm to 12 cm, the horizontal group wall effect coefficient of the model wall increases from 1.09 to 1.16. The horizontal group wall effect coefficients are all greater than 1, and it can be seen from the group wall effect coefficient that an increase in wall height and wall spacing can better exert the horizontal bearing capacity of the wall.

(4) According to the fitting results of  $\beta$ , wall spacing, and wall height, the value range of the group wall effect coefficient is discussed. Based on this, a simplified calculation method of the horizontal load-bearing capacity of the SUDW foundation is proposed, which is made of plexiglass material, and the cap is flush with the sand surface.

**Author Contributions:** Methodology, M.Z.; investigation, W.S.; resources, G.D.; writing—original draft preparation, S.X. and C.L.; writing—review and editing, G.D., X.L., M.Z. and S.L.; supervision, M.Z. All authors have read and agreed to the published version of the manuscript.

**Funding:** This research was funded by the Postgraduate Research & Practice Innovation Program of Jiangsu Province grant number KYCX22-3829; the National Natural Science Foundation of China (52201324); and the Major Basic Research Project of the Natural Science Foundation of the Jiangsu Higher Education Institutions (22KJB560015). The authors are grateful for their support.

**Data Availability Statement:** The data are contained within this article.

**Conflicts of Interest:** Authors Guoqing Du, Weian Shi and Shouguo Li were employed by the company China Energy Engineering Group Anhui Electric Power Design Institute Co., Ltd. The remaining authors declare that the research was conducted in the absence of any commercial or financial relationships that could be construed as a potential conflict of interest.

## References

1. Zeng, C.F.; Zheng, G.; Zhou, X.F.; Xue, X.L.; Zhou, H.Z. Behaviours of wall and soil during pre-excavation dewatering under different foundation pit widths. *Comput. Geotech.* **2019**, *115*, 103169. [[CrossRef](#)]
2. Zhou, N.; Vermeer, P.A.; Lou, R.; Tang, Y.; Jiang, S. Numerical simulation of deep foundation pit dewatering and optimization of controlling land subsidence. *Eng. Geol.* **2010**, *114*, 251–260. [[CrossRef](#)]
3. Zhang, X.; Ou, X.; Yang, J.; Fu, J. Deformation response of an existing tunnel to upper excavation of foundation pit and associated dewatering. *Int. J. Geomech.* **2017**, *17*, 04016112. [[CrossRef](#)]
4. Zhang, J.; Xie, R.; Zhang, H. Mechanical response analysis of the buried pipeline due to adjacent foundation pit excavation. *Tunn. Undergr. Space Technol.* **2018**, *78*, 135–145. [[CrossRef](#)]
5. Zhang, X.; Yang, J.; Zhang, Y.; Gao, Y. Cause investigation of damages in existing building adjacent to foundation pit in construction. *Eng. Fail. Anal.* **2018**, *83*, 117–124. [[CrossRef](#)]

6. Tan, Y.; Wang, D.L. Characteristics of a large-scale deep foundation pit excavated by the central-island technique in shanghai soft clay. I: Bottom-up construction of the central cylindrical shaft. *J. Geotech. Geoenvironmental Eng.* **2013**, *139*, 1875–1893. [[CrossRef](#)]
7. Zheng, G.; Lei, Y.; Cheng, X.; Cheng, X.; Li, X.; Yu, D. Experimental study on the effect of local failure on the support system of steel braced pile rows for foundation pit. *Chin. J. Geotech. Eng.* **2019**, *41*, 1390–1399.
8. Japan Institute of Civil Engineering. *Construction Method of Continuous Wall Foundation in the Ground (Design Compilation)*; Japan Institute of Civil Engineering: Tokyo, Japan, 1994.
9. Japan Institute of Civil Engineering. *Construction Method of Continuous Wall Foundation (Construction Compilation)*; Japan Institute of Civil Engineering: Tokyo, Japan, 1994.
10. Liu, M.; Fu, Y. Design and application of shaft type underground diaphragm wall foundation. *Highway* **2006**, 52–56.
11. Zhang, X.; Wang, S.; Liu, H.; Cui, J.; Liu, C.; Meng, X. Assessing the impact of inertial load on the buckling behavior of piles with large slenderness ratios in liquefiable deposits. *Soil Dyn. Earthq. Eng.* **2024**, *176*, 0267–7261. [[CrossRef](#)]
12. Takuya, K.; Ryo, O. On-site horizontal load test for continuous and intermediate duty の Shaft design method と . *Civ. Eng.* **1980**, *36*, 48–57.
13. James, A.; Kurian, B. Diaphragm wall retaining system—a simplified model for design loads. *Aust. J. Civ. Eng.* **2022**, *20*, 374–388. [[CrossRef](#)]
14. Kawa, M.; Puła, W.; Truty, A. Probabilistic analysis of the diaphragm wall using the hardening soil-small (HSs) model. *Eng. Struct.* **2021**, *232*, 111869. [[CrossRef](#)]
15. Meng, F.; Li, T.; Chen, X.; Gong, W. Experimental study on horizontal bearing characteristics of a single diaphragm wall in loess area. *J. Civ. Eng.* **2006**, *39*, 96–100.
16. Chen, X.; Chai, J. Analysis on bearing behavior of closed diaphragm wall foundation under horizontal load in loess area. *J. Eng. Geol.* **2008**, *16*, 427–431.
17. Zhang, K.; Zhang, M.; Sun, B.; Li, F.; Jian, Y. Deformation calculation method of narrow and long soft soil deep foundation pit wall considering space-time effect. *Rock Soil Mech.* **2023**, *44*, 2389–2399.
18. Li, C. Research on Displacement of Large T-Section Ground Wall Quay and Its Anchorage. Master's Thesis, Tianjin University, Tianjin, China, 2012.
19. Liu, M. Development and prospect of Bridge diaphragm wall foundation. *J. Chongqing Jiaotong Univ. Nat. Sci. Ed.* **2021**, *40*, 41–51.
20. He, H.; Wang, S.; Shen, W.; Zhang, W. The influence of pipe-jacking tunneling on deformation of existing tunnels in soft soils and the effectiveness of protection measures. *Transp. Geotech.* **2023**, *42*, 2214–3912. [[CrossRef](#)]
21. Li, J.; Zhang, Y.; Lin, L.; Zhou, Y. Study on the shear mechanics of gas hydrate-bearing sand-well interface with different roughness and dissociation. *Bull. Eng. Geol. Environ.* **2023**, *82*, 404. [[CrossRef](#)]
22. Dai, G.; Zhou, X.; Liu, Y.; Liu, L.; Gong, W. Model test study on horizontal bearing capacity of downhole diaphragm wall. *Rock Soil Mech.* **2011**, *32*, 185–189+197.
23. Yin, L.; Wang, L.; Li, J.; Lu, S.; Tian, J.; Yin, Z.; Liu, S.; Zheng, W. YOLOV4\_CSPBi: Enhanced land target detection model. *Land* **2023**, *12*, 1813. [[CrossRef](#)]

**Disclaimer/Publisher's Note:** The statements, opinions and data contained in all publications are solely those of the individual author(s) and contributor(s) and not of MDPI and/or the editor(s). MDPI and/or the editor(s) disclaim responsibility for any injury to people or property resulting from any ideas, methods, instructions or products referred to in the content.